International Journal of Biological Macromolecules xxx (xxxx) 127572

Contents lists available at ScienceDirect

International Journal of Biological Macromolecules

journal homepage: www.elsevier.com/locate/ijbiomac

Structural and dynamical changes of the *Streptococcus gordonii* metalloregulatory ScaR protein induced by Mn^{2+} ion binding

Katarina Radman [a], Zoe Jelić Matošević [a], Dijana Žilić [b], Ivo Crnolatac [c], Nikola Bregović [a], Marina Kveder [b], Ivo Piantanida [c], Pedro A. Fernandes [d], Ivana Leščić Ašler [b], Branimir Bertoša [a, *]

[a] Department of Chemistry, Faculty of Science, University of Zagreb, Horvatovac 102a, 10000 Zagreb, Croatia
[b] Division of Physical Chemistry, Ruđer Bošković Institute, 10000 Zagreb, Croatia
[c] Division of Organic Chemistry & Biochemistry, Ruđer Bošković Institute, 10000 Zagreb, Croatia
[d] LAQV, REQUIMTE, Department of Chemistry and Biochemistry, Faculty of Science, University of Porto, Rua do Campo Alegre s/n, 4169-007 Porto, Portugal

ARTICLE INFO

Keywords:
Transcriptional factor ScaR
Metalloregulatory proteins
Allostery

ABSTRACT

Divalent metal ions are essential micronutrients for many intercellular reactions. Maintaining their homeostasis is necessary for the survival of bacteria. In *Streptococcus gordonii*, one of the primary colonizers of the tooth surface, the cellular concentration of manganese ions (Mn^{2+}) is regulated by the manganese-sensing transcriptional factor ScaR which controls the expression of proteins involved in manganese homeostasis. To resolve the molecular mechanism through which the binding of Mn^{2+} ions increases the binding affinity of ScaR to DNA, a variety of computational (QM and MD) and experimental (ITC, DSC, EMSA, EPR and CD) methods were applied. The computational results showed that Mn^{2+} binding induces a conformational change in ScaR that primarily affects the position of the DNA binding domains and, consequently, the DNA binding affinity of the protein. In addition, experimental results revealed a 1:4 binding stoichiometry between ScaR dimer and Mn^{2+} ions, while the computational results showed that the binding of Mn^{2+} ions in the primary binding sites is sufficient to induce the observed conformational change of ScaR.

1. Introduction

Streptococcus gordonii is a nonpathogenic bacterium and one of the primary colonizers of the tooth surface. The metabolic production of hydrogen peroxide produced by *S. gordonii* can inhibit the growth of *Streptococcus mutans*, the primary causative agent of human dental caries [1]. Although commonly considered commensal, *S. gordonii* has been implicated in some cases of apical periodontitis and infective endocarditis [2,3]. Oral bacteria, including *S. gordonii*, can enter the bloodstream not only during invasive procedures, such as oral surgeries, but also during daily activities such as brushing and flossing. Furthermore, *S. gordonii* binds to the cell surface of various host cells, contributing to the initiation of diseases caused by inflammatory responses [2,4]. The adhesion of streptococcal bacteria to the surface of host cells and other bacteria cells in the environment is mediated, for the most part, by cell surface proteins that belong to the LraI family [5–7]. In *S. gordoniii*, the LraI protein is a prominent surface antigen, referred to as ScaA [5]. The gene encoding the ScaA protein (*scaA*) is part of the scaCBA operon consisting of three genes which are transcribed from a promotor upstream of the *scaC* gene. The *scaC* gene encodes an ATP-binding protein while *scaB* encodes a manganese ion (Mn^{2+}) import system permease protein ScaB [5,8]. These three proteins are part of a high-affinity Mn^{2+} transport system in *S. gordonii* that is necessary for cell growth in a low-Mn^{2+} concentration environment and for DNA-mediated transformation [5,9].

Metal ions are essential micronutrients for many intracellular reactions; however, metal excess can be toxic. In bacteria, metal limitation activates pathways for import and mobilization of metals, whereas metal excess induces efflux and storage of the same [10]. The divalent manganese (Mn^{2+}) cation has a variety of important roles in bacterial cells. Depending on the environmental condition and bacterial species, Mn^{2+} ions can function as a cofactor for diverse enzymes in carbon metabolism, nucleotide metabolism, translation and signaling, or they can associate intracellularly with metabolites, proteins and nucleic acids

* Corresponding author.
E-mail addresses: kradman@chem.pmf.hr (K. Radman), zoejm@chem.pmf.hr (Z.J. Matošević), dzilic@irb.hr (D. Žilić), ivo.crnolatac@irb.hr (I. Crnolatac), nbregovic@chem.pmf.hr (N. Bregović), kveder@irb.hr (M. Kveder), ivo.piantanida@irb.hr (I. Piantanida), pafernan@fc.up.pt (P.A. Fernandes), ivana.lescic.asler@irb.hr (I.L. Ašler), bbertosa@chem.pmf.hr (B. Bertoša).

https://doi.org/10.1016/j.ijbiomac.2023.127572
Received 5 September 2023; Received in revised form 16 October 2023; Accepted 19 October 2023
0141-8130/

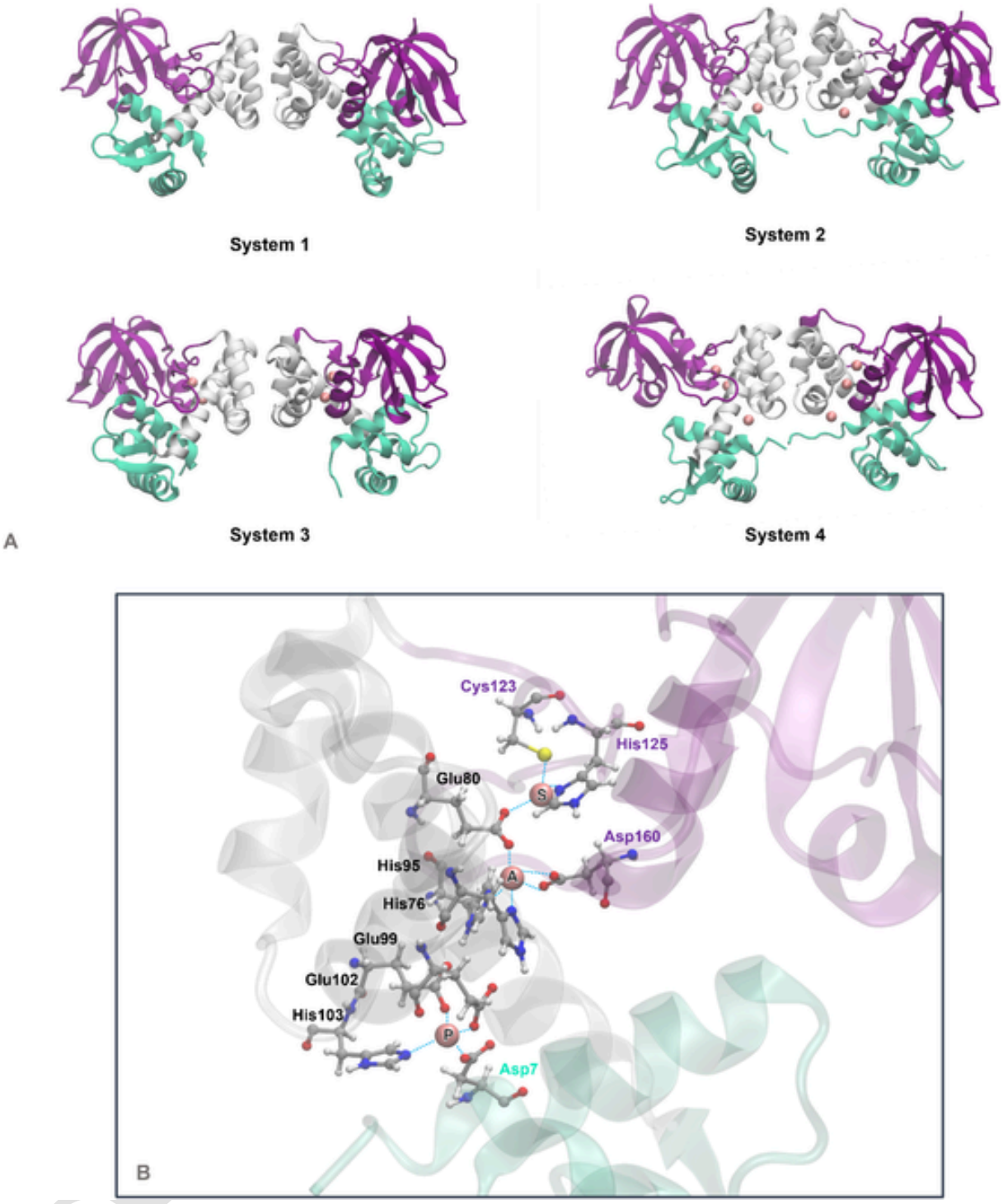

Fig. 1. ScaR protein systems that were subjected to MD simulations. A) System 1 – *apo*ScaR; System 2 – ScaR with Mn^{2+} ions in each primary binding sites; System 3 – ScaR with Mn^{2+} in the ancillary and secondary binding site; System 4 – ScaR with Mn^{2+} in all three binding sites. The DNA binding domains (DBDs) are shown in cyan blue, dimerization domains are shown in white and the SH3 like domains are shown in purple. B) Positions of all three metal binding sites. Residues Asp7, Glu99, Glu102 and His103 form the primary binding site (Mn^{2+} ion labeled as P). Residues His76, Glu80, His95 and Asp160 form the ancillary binding site (Mn^{2+} ion labeled as A). Residues Glu80, Cys123 and His125 form the secondary binding site (Mn^{2+} ion labeled as S). Water molecules that coordinate Mn^{2+} ions are not shown. (For interpretation of the references to color in this figure legend, the reader is referred to the web version of this article.)

[11]. Both manganese deficiency and toxicity are key problems that bacteria must avoid. Manganese homeostasis in bacteria is maintained by the expression and activity of Mn^{2+} import and export machinery. The transcription of Mn^{2+} export and import machinery is under the control of transcriptional factors and RNA-mediated elements that can post-transcriptionally modulate gene expression [10,11]. In *S. gordonii*, the homeostasis of Mn^{2+} ions is regulated by the manganese-sensing transcriptional factor ScaR which controls the expression of the previously mentioned scaCBA operon [8]. When intracellular manganese concentration becomes elevated, ScaR binds to the scaCBA promotor and represses the expression of the scaCBA operon, which encodes the manganese import system permease protein ScaB [5,8,9].

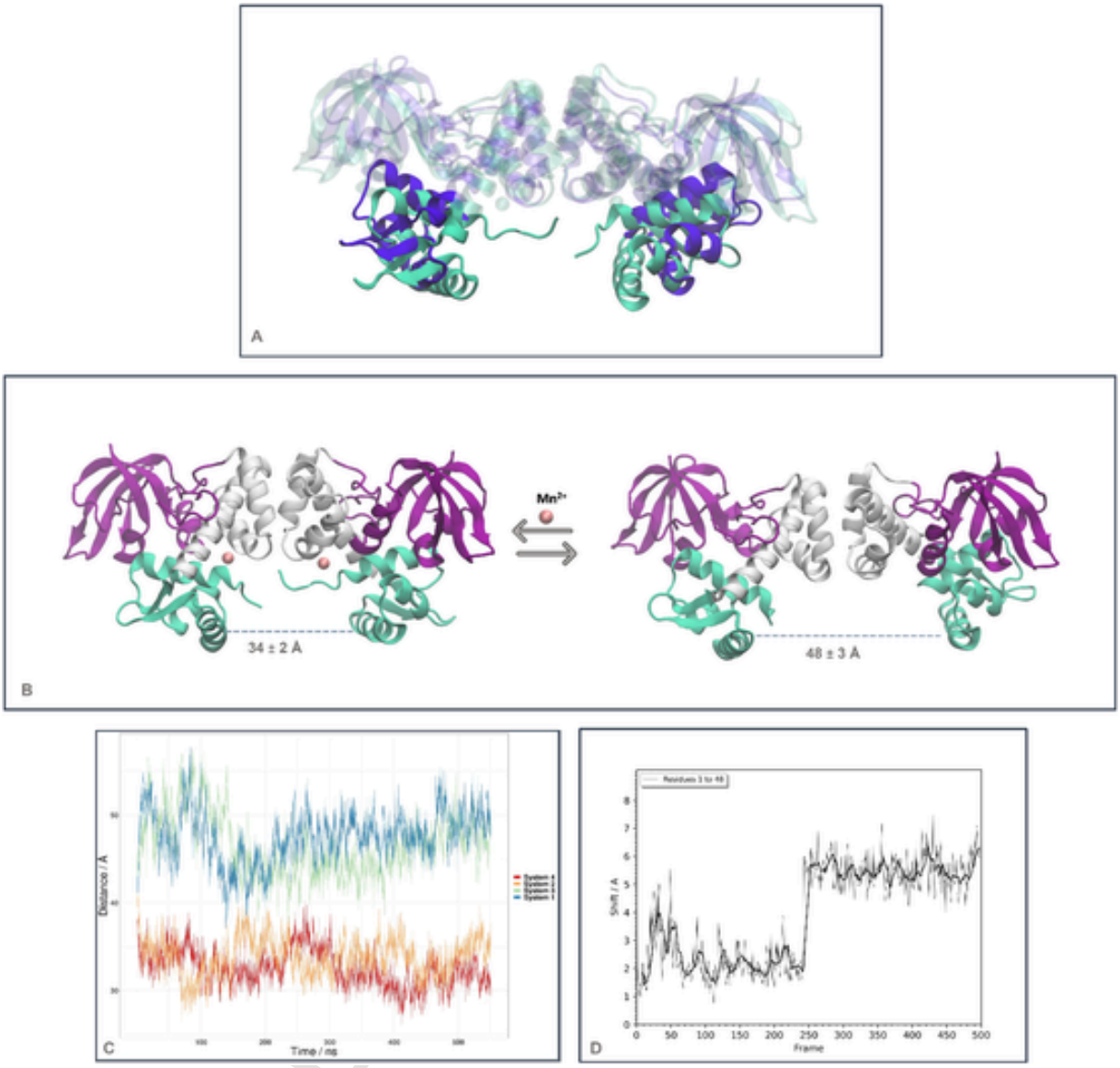

Fig. 2. Movement of the DNA binding domains (DBDs). A) Superimposed structures of the centroid of the most-populated cluster for simulations of System 1 (cyan) and System 2 (blue). The DBDs are opaque while the rest of the protein is transparent. B) Removal of the Mn2+ ion from the primary binding site causes movement of the DBDs away from each other. C) Distance between the α2 helix during the MD simulations of all four systems (α2 helix was defined as all atoms between residues 23 to 30 for both monomers). D) Movement (shift) of the DBD during the MD simulation of the apo system (System 1) – position of the DBDs of each frame was compared to the structure in the first. The shift was quantified using TrajMap.py (available at https://github.com/matkozic/TrajMap). (For interpretation of the references to color in this figure legend, the reader is referred to the web version of this article.)

ScaR, together with its streptococcal homologs, belongs to the streptococcal clade of the DtxR/IdeR family of Fe^{2+}- and Mn^{2+}- regulated repressors that control the transcription of ABC metal ion transporters [9,12–15]. Crystallographic studies of the DtxR protein (*Corynebacterium diphtheriae*) have shown that the active form of the repressor is a homodimer in which each monomer is composed of three domains: an N-terminal winged helical DNA-binding domain, a central dimerization domain promoting quaternary structure, and a C-terminal domain that has a fold similar to the Src homology 3 (SH3, also known as FeoA) domain [15,16]. DtxR requires metal binding to a pair of ancillary sites near the C-terminal SH3-like domain to induce protein dimerization. Subsequently, the binding of a pair of metal ions to the regulatory, so-called primary site, allosterically activates the protein for DNA binding and promotes transcriptional repression [15]. Members of the streptococcal clade of DtxR/IdeR, including ScaR, preserve the three-domain structure of DtxR and many of the residues in the primary metal binding site found in DtxR, but these proteins form stable homodimers in solutions while DtxR is a monomer [9,12,14,15,17]. The selectivity of ScaR for manganese over iron is based on ligand selection [18]. The primary binding site of DtxR consists of two sulfur-containing residues, Met10 and Cys102, while in the ScaR protein, residues Asp7 and Glu99 are in analogous positions. Previous research suggests that no known proteins selective for Mn^{2+} ions use sulfur atoms as ligands [18,19]. Furthermore, crystallographic studies of ScaR, SloR (*S. mutans*) and MtsR (*S. pyogens*) proteins showed another binding site closer to the SH3-like domain, referred to as the secondary binding site, that is distinct from the known ancillary site in DtxR [9,13,14]. Although it is possible that the observation of divalent metal ions in the secondary binding site of ScaR is an artefact of crystallization conditions, the broad conservation of potential metal binding residues at the appropriate positions across the DtxR/IdeR family and the observation that ScaR binds two to three metal ions per subunit suggest that metal binding at this site could fulfill a selected function [9].

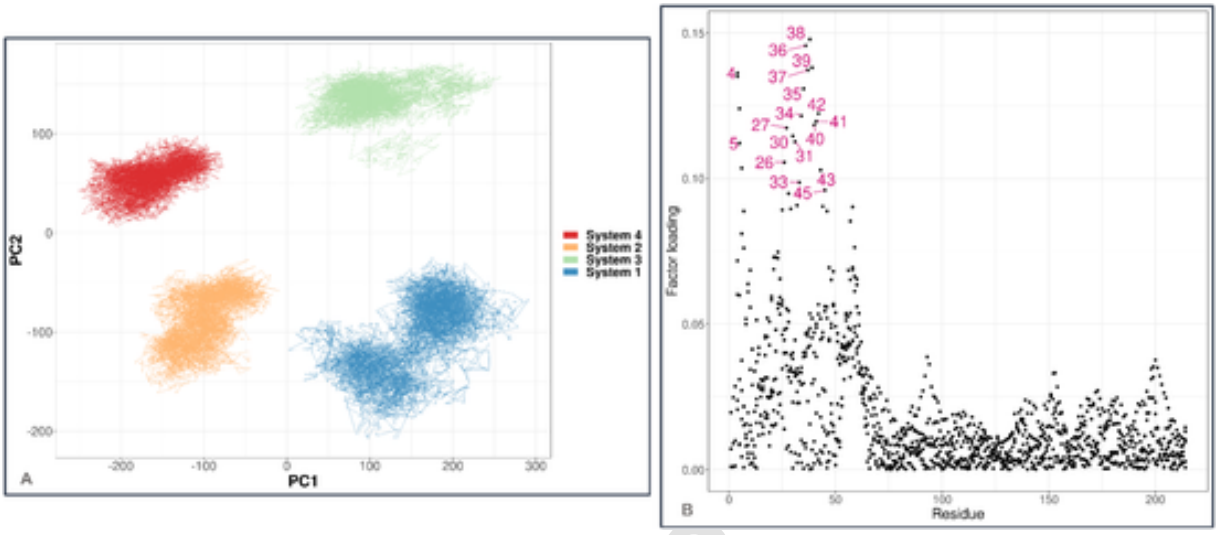

Fig. 3. Principal component analysis of MD simulations. A) The principal component projection of all four systems on PC1 and PC2. B) Factor loading for PC1 – the labeled points represent the main contributors to the variance in PC1.

The goal of the present study was to further advance the understanding of the structural and dynamical changes of the ScaR protein that occur upon binding of Mn^{2+} ions. In this regard, several ScaR-Mn^{2+} ion complexes were investigated using molecular dynamics simulations. Along with computational research, laboratory experiments were performed. The change in overall protein structure and stability upon binding of Mn^{2+} was monitored using circular dichroism (CD) followed by differential scanning calorimetry (DSC). The binding thermodynamics and stoichiometry were determined using isothermal titration calorimetry (ITC). Additionally, the presence of ScaR-Mn^{2+}complexes and their binding stoichiometry were confirmed by means of EPR studies.

2. Materials and methods

2.1. Molecular dynamics simulations

2.1.1. System preparation and parametrization

Four systems of the ScaR protein were prepared for molecular dynamics (MD) simulations: (i) *apo* (System 1 – without Mn^{2+} ions), (ii) Mn^{2+} ion in each primary binding site (System 2 – two Mn^{2+} ions per homodimer), (iii) Mn^{2+} ions in the ancillary and secondary binding sites (System 3 – four Mn^{2+} ions per homodimer), (iv) Mn^{2+} ions in all binding site (System 4 – six Mn^{2+} ions per homodimer) (Fig. 1). All systems were prepared from the same starting crystal structure of the ScaR protein bound to Cd^{2+} ions (PDB id: 3HRT [9]) The structure was missing residues Thr2-Pro3-Asn4-Lys5 [9] in one monomer and it was completed using the protein structure homology modelling server SWISS-MODEL [20] and Pymol Molecular Graphic System [21]. Hydrogen atoms were added using the H + + web server [22] at pH 7.0, which is the average pH of the oral cavity [23]. The protonation of residue His95 was edited manually to assure subunit symmetry in the homodimer. The position of the Mn^{2+} ion binding sites was based on the crystal structure of the homologous metalloregulatory protein SloR with Zn^{2+} ions bound (PDB id: 5CVI [13]). SloR shares 86 % similarity (based on BL80 [24]) with ScaR and the predicted metal binding sites are the same [9,13].

Parametrization of the interaction between the protein and Mn^{2+} ions for the primary (mononuclear) binding site was made separately from the ancillary and secondary binding sites, which were parameterized together as a binuclear binding site because they share a ligand. All binding sites were parametrized using a bonded model. The geometries of the metal binding centers were optimized using Gaussian 16 rev. B.01, at the unrestricted UB3LYP/aug-cc-pVDZ level of theory with Grimme's empirical correction for dispersion (GD3) and all computations were performed in solvent (water) using the Polarizable Continuum Model (PCM). Single point frequency calculations were performed on the optimized structures in Gaussian at the same level of theory. Next, using the VFFDT software [25], force field parameters for bonds and angles were taken out from the frequency calculations. To complete the metal centers parameterization, charges were calculated using the Merz-Singh-Kollman scheme [26] in Gaussian16 and the RESP approach [27] was used to calculate the final atomic charges. Lennard-Jones parameters were taken from the Li/Merz ion parameters for Mn^{2+} in TIP3P water [28].

The remaining parts of the systems were parametrized using the Amber ff14SB force field and the TIP3P water model. System topology files were obtained using the *tleap* program (Amber20 packages). Periodic boundary conditions were applied using a cubic water box around the protein. The distance between protein atoms and the edge of the box was 20 Å. Systems were neutralized with sodium ions.

2.1.2. Molecular dynamics simulations

All computational simulations were conducted using the Amber20 software [29–32]. Prior to MD simulations, all systems were energy minimized in 5 cycles each consisting of 1000 steps. The first 200 steps of energy minimization (geometry optimization) were performed using the steepest descent, and the next 800 steps using the conjugate gradient algorithm. In the first cycle all protein atoms and Mn^{2+} ions were restrained with a harmonic potential of 100 kcal/(molÅ^2). In the second cycle, protein heavy atoms and Mn^{2+} ions were restrained using the same potential. In the third and fourth cycles, protein backbone atoms were restrained, in the third cycle with harmonic potential of 100 kcal/(molÅ^2) and in the fourth with a potential of 50 kcal/(molÅ^2). In the fifth cycle the systems were minimized without any restraints. After energy minimization, systems were equilibrated. Through the first 250 ps of the equilibration simulations the temperature was linearly increased from 0 K to 310 K, while from 250 ps to 300 ps the temperature was kept constant (canonical NVT ensemble) using a Langevin thermostat [33] with collision frequency set to 1 ps^{-1}. The volume of the systems was kept constant, and water (solvent) atoms were restrained using a harmonic potential with a force constant of 32 kcal/(molÅ^2). During the next 200 ps, the systems were equilibrated at a constant temperature (310 K) and pressure (1 bar) (NPT ensemble) using the Langevin thermostat with the collision frequency set to 2 ps^{-1} and isotropic position scaling. Next, during the production phase of MD simulations, sys-

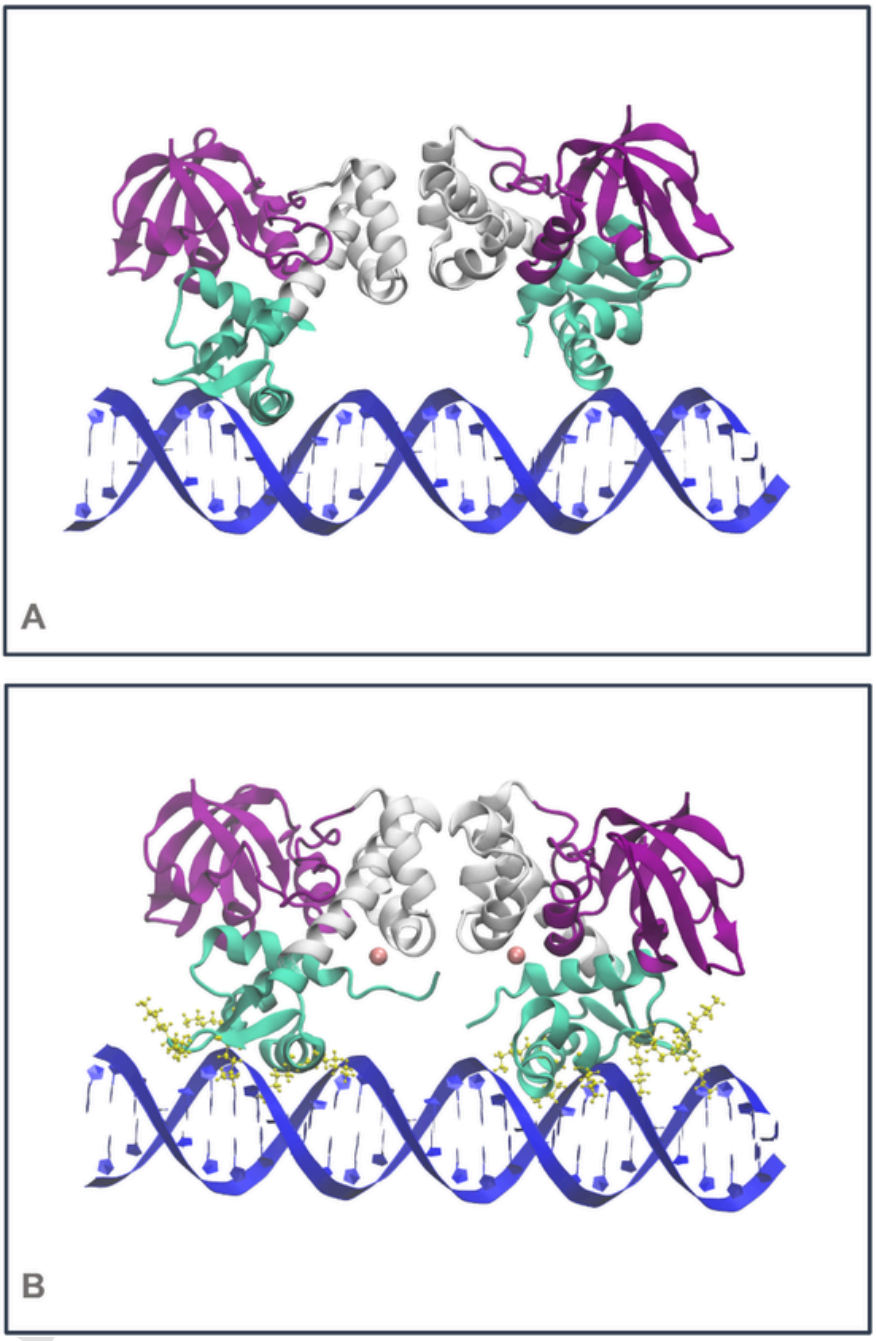

Fig. 4. ScaR-DNA complexes. A) *Apo* ScaR (System 1) shown with the DNA operator element (blue). One DBD is placed in the major groves, but the other cannot fit the neighboring major grove due to interdomain distance between DBDs. B) ScaR with Mn^{2+} ions in each primary binding site (System 2) shown with the DNA operator element (blue). The DBD domains are at the appropriate distance to fit the neighboring major groves. Lysine residues of the DBD helices are shown in yellow. DNA binding domains (DBDs) are shown in cyan blue, dimerization domains are shown in white and the SH3 like domains are shown in purple. (For interpretation of the references to color in this figure legend, the reader is referred to the web version of this article.)

tems were subjected to 550 ns of simulations. The production phase was performed in the NPT ensemble at T = 310 K, which was maintained using the Langevin thermostat with the collision frequency set to 1 ps^{-1}. The time step of the simulations was 1 fs and every 100 ps structures were written to a trajectory file. Periodic boundary conditions (PBC) were imposed in all three directions, with long range electrostatic interactions calculated by the particle-mesh Ewald (PME) method [34].

2.1.3. Analysis of simulations

Trajectory analyses such as RMSD (Fig. S1 in SI), RMSF, radius of gyration, distances between amino acids or protein domains, as well as principal component analysis (PCA) were performed using the *cpptraj* program (Amber20 program package) [29]. To perform the PCA analysis, the trajectories were stripped of the first and last three residues in each chain because they show significantly higher fluctuations than other residues and create noise in the data. PCA was performed on the last 500 ns of the 550 ns production phase for all four systems. Trajectories were merged and then covariance matrices on the Cartesian coordinates of the Cα protein backbone atoms were calculated. Factor load-

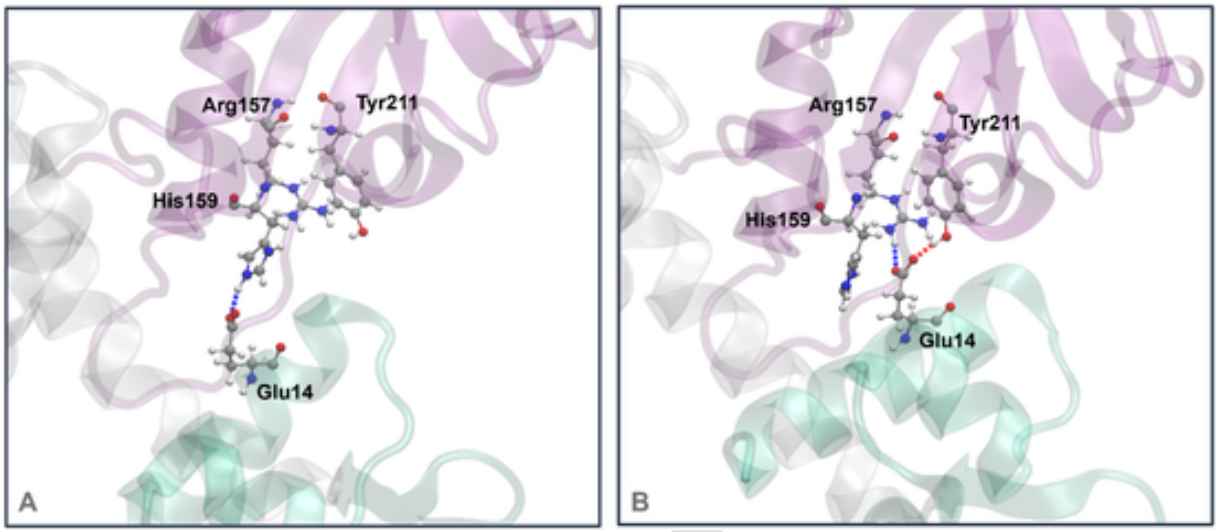

Fig. 5. Hydrogen bonds between the α1 helix and the SH3-like domain of System 1: A) at the beginning, and B) at the end of the MD simulations. Glu14 belongs to α1 helix, Arg157, His159 and Tyr211 belong to the SH3-like domain. DNA binding domain is shown in cyan blue, dimerization domain is shown in white and the SH3 like domain is shown in purple. (For interpretation of the references to color in this figure legend, the reader is referred to the web version of this article.)

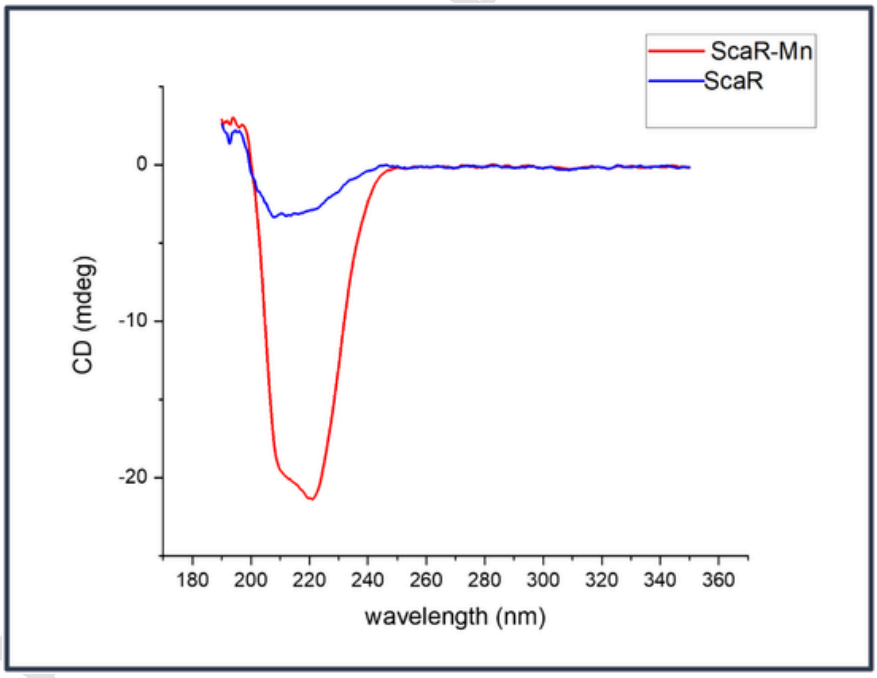

Fig. 6. Raw CD spectra of ScaR protein in 20 mM Hepes buffer pH 8.0 containing 100 mM NaCl, with and without the addition of Mn^{2+}.

ing analysis was made using RStudio [35] to determine which residues are the main contributors to the variance in the dominant principal component vector (PC1).

The raw data was processed and plotted using the data.table [36] and ggplot2 [37] packages in R. Trajectories and pdb structures were visualized using VMD [38] and Maestro [39]. For more elaborate analyses of the system dynamics, trajectory heatmaps were made using a program developed within our research group [40].

2.1.4. Preparation of the DNA-protein system

To analyze the interactions between protein and DNA, the ScaR binding site of the scaCBA operon promoter region (5′-CAAAATTAACTTGACTTAATTTTG-3′) [8] was built *in situ* using Maestro [39]. The initial coordinates of the protein were taken from the last frame of the previous 550 ns MD simulation. The template of the DNA-protein system was based on the structure of DNA-protein complexes from homologous proteins [14,41]. The interactions were analyzed using Maestro and VMD.

2.2. Protein cloning, expression and purification

Plasmid *N-His_SScaR_pET-45b(+)* containing the gene for full-length ScaR protein from *Streptococcus gordonii* was purchased from GenScript Biotech (Leiden, The Netherlands). The plasmid contains a fusion tag sequence coding for 6 His and the cleavage site for HRV-3C protease added at the protein's N-terminal. The plasmid was subcloned into *E. coli* cell strain BL21-CodonPlus (DE3)-RIL (Agilent Biotechnology, USA) using electroporation. The expression of the protein was performed in LB medium containing 100 μg/mL of ampicillin. The cell culture was incubated at 37 °C and 140 rpm for 3 h to OD_{600nm} ~ 0.6 at

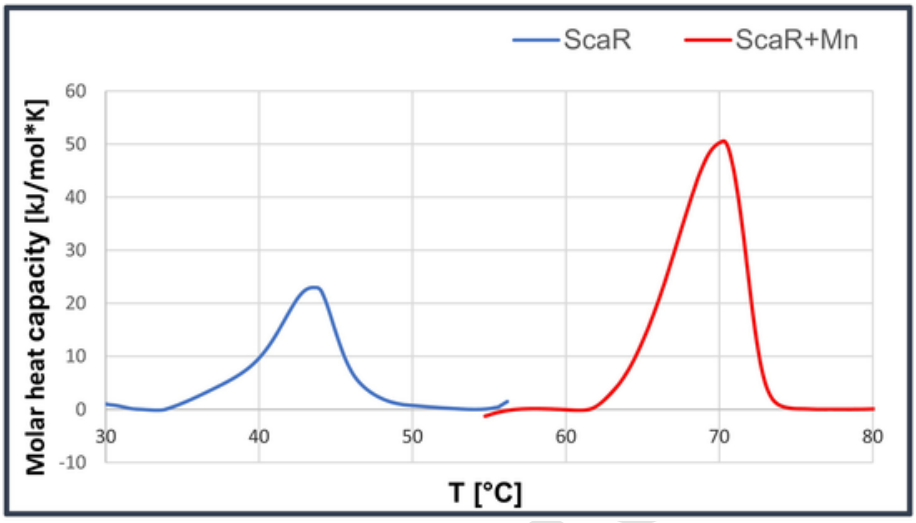

Fig. 7. DSC Thermograms, represented as baseline subtracted molar heat capacity traces of 2 mg/mL *apo*ScaR and ScaR-Mn^{2+} complex.

Table 1
Thermal unfolding characteristics of ScaR proteins, extracted from the DSC scans: Temperature (T_m/°C) and enthalpy (ΔH/kJ·mol^{-1}).

Sample	γ (mg/mL)	*Mw* (kDa)	T_m (K)	ΔH_m (kJ/mol)
ScaR	2	25	316.78	136.83
ScaR-Mn^{2+}	2	25	343.38	280.29

which time IPTG (Isopropyl β-D-1-thiogalactopyranoside) was added to 0.5 mM, and the cell cultures were further incubated over-night at 18 °C and 50 rpm. Cells were harvested at 5000 × *g*, at 4 °C.

Protein purification was performed at 4 °C. Cells were resuspended (10 mL/g of cells) in 50 mM Na-phosphate buffer pH 7.0 containing 300 mM NaCl, 10 mM imidazole and 5 % glycerol (buffer A). PMSF was also added to the concentration of 0.1 mM, and the cells were lysed using a high-pressure homogenizer (Avestin Emulsiflex C3, Canada). Cell debris was separated from protein extract by centrifugation for 45 min at 15,000 × *g* and 4 °C. Protein extract was loaded onto a column of 1.5 mL Ni-NTA agarose (Protino, Macherey-Nagel GmbH & Co. KG) equilibrated in buffer A. The column was washed in two steps – with 10 mL of buffer A and with 10 mL of buffer B (same as buffer A, but with 20 mM imidazole). Bound proteins were eluted with 10 mL of buffer C (same as buffer A but with 300 mM imidazole). During an overnight dialysis the N-terminal His-tag was cleaved off with HRV-3C protease (1 μmol of protease per 30 μmol of protein) (Thermo Scientific, Pierce Biotechnology, Rockford, IL 61105, USA). The dialysis was performed towards 1 L of 50 mM Hepes buffer pH 7.5, containing 150 mM NaCl, 1 mM EDTA, 1 mM 2-mercaptoethanol and 10 % glycerol and after the first 2 h of dialysis the buffer was exchanged with a fresh one because of the high concentration of imidazole in the eluting buffer C. Size-exclusion chromatography (SEC) was performed for additional purification of the protein. HiLoad 16/600 Superdex 75 pg column (Cytiva Life Sciences, United States) was equilibrated in 25 mM Hepes buffer pH 8.0 containing 300 mM NaCl and 10 % of glycerol (SEC buffer) and operated at 1 mL/min on the ÄKTA Pure FPLC system (Cytiva Life Sciences, United States). Two milliliters of the concentrated sample were loaded onto the column, and fractions of 2 mL were collected. Fractions containing purified ScaR were combined and dialyzed over night against 1 L Hepes buffer pH 8.0 containing 100 mM NaCl, with 10 g/L Chelex 100 chelating resin floating free in the buffer. The final sample of purified protein was stored in aliquots at −80 °C until use.

The purification was monitored using electrophoresis under denaturing conditions (SDS-PAGE) and protein concentration was determined at 280 nm utilizing protein's molar extinction coefficient of 16,390 M^{-1} cm^{-1} which was calculated using the ProtParam tool at ExPasy.org [42].

SEC on a HiLoad 16/600 Superdex 75 pg column (under the conditions described) was also used to estimate the molecular mass/

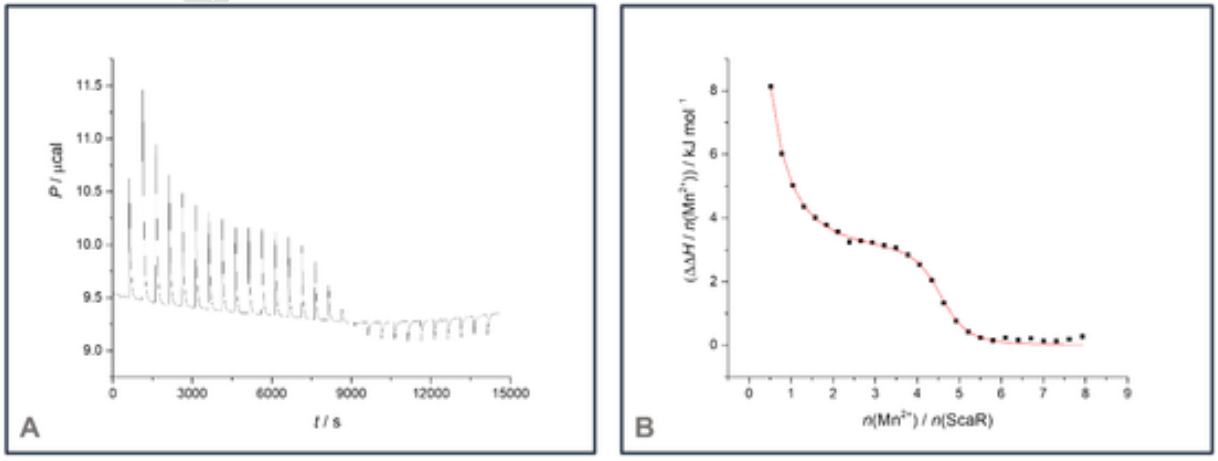

Fig. 8. Microcalorimetric titration (ITC) of ScaR (c = 0.1 mM, V = 1.449 mL) with $MnCl_2$ at pH = 8 (20 mM Hepes buffer, containing 100 mM NaCl) at 25 °C.

Table 2
Thermodynamic parameters for complexation of ScaR dimer ($ScaR_2$) with Mn^{2+}.[a]

Species	log β	K_d/μM	$\Delta_r H°$/kcal mol^{-1}	$\Delta_r S°$/kcal K^{-1} mol^{-1}
$ScaR_2Mn$	5.01(6)	9.7(1)	22.0(6)	96.7
$ScaR_2Mn_2$	10.33(4)	4.79(7)	8.9(1)	77.2
$ScaR_2Mn_4$	20.59(4)	–	19.91(3)	161.0

[a] The uncertainties are expressed as standard deviations.

oligomeric state of ScaR. The column was calibrated with several proteins from the Gel Filtration Molecular Weight Markers kit (Sigma) and the Gel Filtration Calibration Kit (Cytiva) – cytochrome C (12.4 kDa), carbonic anhydrase (29 kDa), ovalbumin (44 kDa), and conalbumin (75 kDa), together with Blue Dextran 2000. Ultraviolet absorption detection at 280 nm was used for determining the elution volume of the marker proteins.

2.3. Circular dichroism measurements

The CD spectra were recorded on a JASCO J-815 spectropolarimeter at room temperature in 20 mM Hepes buffer pH 8.0 containing 100 mM NaCl, using 0.01 cm path quartz cuvettes with a scanning speed of 200 nm/min. The spectra were recorded as a mean value from three scans in the wavelength range 190–300 nm and the buffer spectrum were subtracted. The online service BeStSel [43] (Beta Structure Selection) was used for the secondary structure determination and fold recognition from ScaR CD spectra.

2.4. Differential scanning calorimetry measurements

The DSC measurements were performed on Nano DSC, Differential Scanning Calorimeter (TA Instruments) with a 300 μL cell volume, in the temperature range 20–110 °C and scanning/heating rate of 1 °C/min. The samples were prepared in 20 mM Hepes buffer pH 8.0 containing 100 mM NaCl. Upon buffer against buffer measurement, used for baseline subtraction, the reference cell was filled with buffer and the sample cell with protein (2 mg/mL). The recorded thermograms were analyzed with the NanoAnalyze Data Analysis (Version 3.11.0) software package.

2.5. Isothermal titration calorimetry

ITC measurements were performed by means of isothermal titration microcalorimeter (MicroCal VP-ITC) at 25.0 °C. Origin 7.0 software, supplied by the manufacturer, was used for data acquisition and manipulation. The calorimeter was calibrated electrically. The volume of the calorimeter cells was 1.449 mL, while the total volume of the burette was 0.3 mL. The ITC titrations were carried out by stepwise addition of 1.88 mM $MnCl_2$ solution prepared in 20 mM Hepes buffer pH 8.0 containing 100 mM NaCl to a 0.1 mM solution of ScaR prepared in the same buffer. Constant stirring was applied, and the time between additions was set to 500 s. Blank experiments were carried out to obtain heats of dilution which were subtracted from heat signals measured in the titration experiment. The dependence of the measured enthalpy change on the volume of the added titrant was processed by a non-linear least-squares fitting procedure.

2.6. Electron paramagnetic resonance

Continuous-wave (CW) EPR experiments were performed using an X-band Bruker EMX spectrometer. The spectra were acquired at room temperature using the following set-up parameters: microwave power of 20 mW, modulation amplitude of 0.5 mT, and 100 kHz modulation frequency. The samples (same as for the ITC measurements) were measured in 0.25 μL hematocrit glass capillaries inserted into a quartz tube with an inner diameter of 4 mm.

2.7. Electrophoretic mobility shift assay

The double-stranded DNA sequence of the scaCBA operon promoter region [8] was purchased from Macrogen Europe and dissolved in doubly distilled water giving stock solution of 100 μM. The sequence: 5′-CAAAATTAACTTGACTTAATTTTG-3′. The assay was performed in 20 μL reaction volumes each containing 50 mg/mL BSA (bovine serum albumin), 50 mM NaCl, 1 mM DTT (dithiothreitol) and 5 % glycerol in 10 mM Tris-HCl buffer pH 7.6. Stock solutions of Mn^{2+} ($MnCl_2$) were

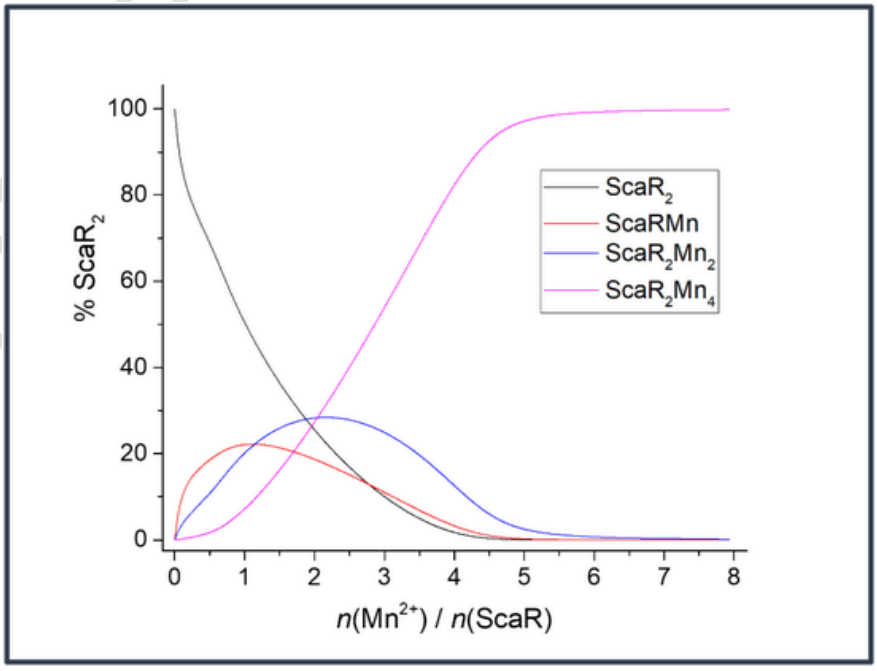

Fig. 9. Distribution diagram of solution containing ScaR and manganese cation in Hepes buffer (pH 8.0) at 25 °C.

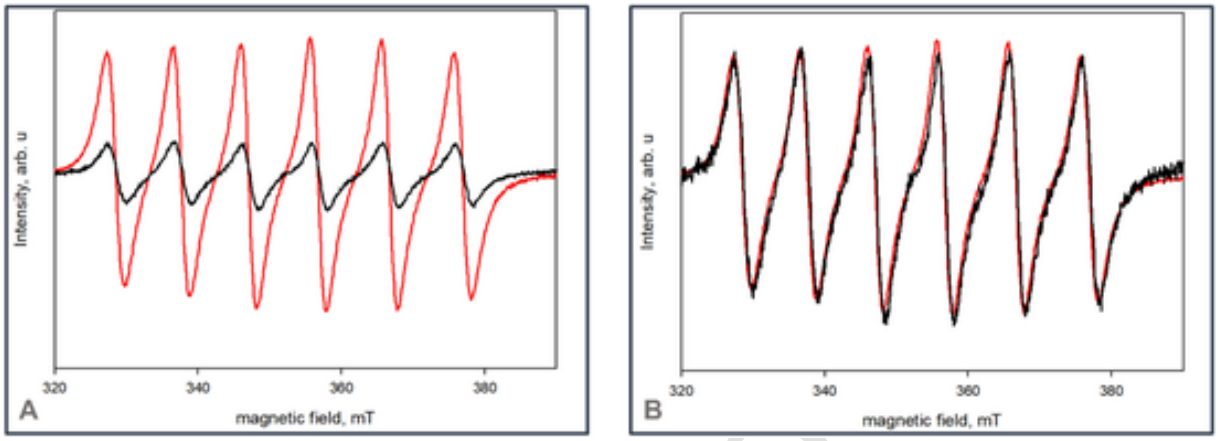

Fig. 10. EPR spectra of 2.7 × 10−4 M concentration of Mn^{2+} in the buffer solution in the absence (red) and in the presence of 8.7 × 10−5 M ScaR (black) measured at room temperature. A) EPR spectra of pure buffer solution containing Mn^{2+} ions (red) and in the presence of protein (black); B) EPR spectrum of Mn^{2+} in the presence of protein scaled with a factor of 4 (black) to match the intensity of Mn^{2+} in the pure buffer solution (red). (For interpretation of the references to color in this figure legend, the reader is referred to the web version of this article.)

prepared fresh before use and added to certain reaction mixtures to the final concentration of 4 mM (or 16 mM in reaction with 8 mM EDTA). DNA was added to the concentration of 5 μM. Protein ScaR was added to the concentration of 100 μM. This ratio of ScaR/DNA ensured complete binding of DNA to the protein. The reactions were incubated at room temperature for 15 min. The samples were dyed with bromophenol blue and 10 μL of each sample was loaded on a 12 % polyacrylamide gel (Mini-PROTEAN® TGX Stain-Free™ Protein Gels, BioRad). The gel was equilibrated prior to sample loading at 100 V and 4 °C for 30 min and the samples were separated at 100 V and 4 °C for 60 min, in TB buffer pH 7.6 (89 mM Tris, 89 mM borate). DNA was visualized in the gel by staining with ethidium bromide.

3. Results and discussion

3.1. Distance between the DBDs is regulated by the presence of Mn^{2+} ions in the primary binding sites

The distance between the two DNA binding domains (DBDs, residues 1 to 63) of the ScaR protein increased during MD simulations of the systems without Mn^{2+} ions bound in the primary binding site (Systems 1 and 3) (Fig. 2). During these simulations (System 1 and 3), the DBD shifted closer to the SH3-like (FeoA) domain which resulted in a larger distance between the DBDs (Fig. 2). The other two systems, System 2 with Mn^{2+} ions present in the primary binding site and System 4 with Mn^{2+} ions bound in all three binding sites, showed the opposite behavior of the DBDs. In Systems 2 and 4, the DBDs moved closer to each other during the simulations (Fig. 2). The difference in the distance between the DBDs of the relaxed systems with and without Mn^{2+} ions in the primary binding site is around 14 Å (Fig. 2). Also, the presence of Mn^{2+} ions in the primary binding sites lowers the fluctuations of the DBDs compared to the systems without Mn^{2+} ions in the primary binding sites (Fig. S2 in SI). Analysis of the trajectories showed that the fluctuations of the DBDs in Systems 1 and 3 are 3.1 ± 0.8 Å, while for Systems 2 and 4 they are 2.1 ± 0.4 Å.

Principal component analysis (PCA) was performed on the Cartesian coordinates of the protein backbone Cα atoms for the last 500 ns of simulation time. The first principal component (PC1) describes 92 % of variance in all simulations, while the second (PC2) describes 5 % and the third (PC3) 2 % of variance. The PC projection of all four systems on PC1 and PC2 showed a clear separation between the systems with and without Mn^{2+} ions in the primary binding site (Fig. 3A). In other words, the variance in PC1 reflected the difference between the simulations of the four systems and identified the residues at the DBD as the main contributors to these differences, in particular residues 4 to 45 of both DBDs (Fig. 3B).

Furthermore, relaxed protein structures (the last frame of the MD simulation) of four systems were used to generate *in silico* ScaR-DNA complexes. The DBDs of the ScaR protein of the systems with Mn^{2+} ions in the primary binding site (System 2 and 4) easily fitted into the major grooves of the scaCBA operon promoter region. The DBDs in Systems 2 and 4 are at an appropriate distance to fit the adjacent DNA grooves (Fig. 4). In addition, the Lys residues – 43, 44, 53, 55, 56 of the DBDs are in a favorable position to form interaction with the DNA backbone (Fig. 4B). On the other hand, in Systems 1 and 3 the DBDs are further apart from each other and cannot fit into the DNA grooves (Fig. 4).

3.2. A molecular mechanism through which the presence or absence of Mn^{2+} ions in the primary binding site regulates the distance between the DBDs

The molecular mechanism through which the presence or absence of Mn^{2+} ion in the primary binding site regulates the distance between the DBDs was elucidated from the analysis of MD simulations. The presence or absence of Mn^{2+} ions in the primary binding sites regulates movement of the α1 helices, which consequently affects the distance between the DBDs.

During the simulations of Systems 2 and 4, the position of the α1 helices was held in place due to the presence of permanent bonds between Mn^{2+} ions in the primary binding sites and Asp7 of the α1 helix. The distance between the α1 helix and the SH3-like domain, as well as the hydrogen bond between Glu14 of the α1 helix and His158 of the SH3-like domain, were constant during the simulations (Fig. 5A). The inability of α1 helices to move induced a shift of the DBDs closer to each other (Fig. 2).

On the other hand, the absence of Mn^{2+} ions in the primary binding site in System 1 and 3, caused a shift (Figs. S3 and S4 in SI) of the α1 helix closer to the SH3 domain in both monomers, which resulted in an increase in the distance between the DBDs during the MD simulations (Fig. 2). The movement of the DBDs was accompanied with the rearrangement of interactions between the α1 helix and SH3-like domain (Figs. 2 and 5). At the beginning of the simulations, Glu14 of the α1 helix was forming a hydrogen bond with His158 of the SH3-like domain (Fig. 5A). After 250 ns of MD simulations of System 1, the hydrogen bond between Glu14 and His158 broke because of the shift of the α1 helix towards the SH3-like domain. New hydrogen bonds between Glu14 of the α1 helix on one side, and Arg156 and Tyr211 of the SH3-like do-

main, were formed and kept constant until the end of simulations (Fig. 5B and Fig. S5 in SI).

3.3. The stability of the ScaR protein is enhanced in the presence of Mn^{2+} ions

The *scaR* gene was successfully expressed in *E. coli* and typically yielded ~20 mg of native ScaR protein from 1.5 L of culture, purified by two chromatography steps. Final preparation, after treatment with Chelex resin, appeared homogeneous on a SDS-PAGE, with a molecular weight of 26.3 kDa for a monomeric unit (Fig. S6 in SI). Elution volume (54.41 mL) from a size-exclusion chromatography column corresponds to a molecular weight of ~63 kDa indicating dimeric state of the protein, in given conditions, within the accuracy of the method (Fig. S7 in SI). The functionality of the purified ScaR protein, its binding to palindromic operator element in the presence of Mn^{2+}, was confirmed by EMSA (Fig. S8 in SI). Observed formation of ScaR/DNA complex even in the absence of Mn^{2+} might be consequence of short DNA sequence (24 bp) used in the experiments. The conformational analysis of the ScaR protein and its Mn^{2+} complex from CD spectroscopy (Fig. 6) confirms that the protein is stable at 4 °C and that it predominantly has a helical structure (Fig. S9 in SI). Upon Mn^{2+} binding, the secondary structure could not be deconvoluted by BeStSel service.

DSC thermograms reveal the influence of Mn^{2+} binding on the thermodynamics of the unfolding process and the thermal stability of ScaR (Fig. 7). The results show that the enthalpy of the unfolding process of *apo*ScaR was 136.83 kJ/mol and it increased considerably up to 280.29 kJ/mol upon Mn^{2+} complexation. Similarly, the unfolding temperature (T_m) increased dramatically from 43.63 °C to 70.23 °C (Table 1). Previous research has confirmed that the observed stabilization is specific to activation by transition metal ions [18,41,44].

3.4. ScaR binds four Mn^{2+} per protein dimer

The ITC titration curve featured a complex shape clearly suggesting an elaborate binding sequence including several complex species present in equilibrium (Fig. 8A). Strong endothermic signals were detected at low Mn:$ScaR_2$ molar ratio, which rapidly declined as 1:1 M ratio was achieved. This was followed by a plateau in the titration curve until roughly 4 equivalents of Mn^{2+} (in relation to ScaR dimer) were added. With further addition of the cation, the heat signals decayed in a sigmoidal fashion becoming negligible after addition of 5 Mn^{2+} equivalents.

The best fit of the acquired experimental data could be achieved by assuming binding of 1, 2 and 4 Mn^{2+} to a ScaR dimer ($ScaR_2$) (Fig. 8B) using HypDH program for data processing. The stability constants of the formed complexes *i.e.* the cumulative association constants (β), were thus reliably determined, and their logarithmic values are provided in Table 2. In addition, the corresponding dissociation constants (K_d) were calculated where applicable to aid the comparison with other similar systems. The reaction enthalpies and entropies given in Table 2 are all related to complex formation, starting from free Mn^{2+} cation and $ScaR_2$ dimer.

All processes were found to be endothermic (complex formation from free Mn^{2+} and $ScaR_2$) and entropically favored, most likely reflecting the strong desolvation of the protein and the cation upon binding of Mn^{2+} and, potentially, loss of favorable intramolecular interactions within the protein free form. The highest reaction enthalpy was measured for the formation of the monocationic complex. This complex is favored at low Mn^{2+}:ScaR molar ratio causing the heat signals measured upon first few additions of Mn to be rather high. The binding of the second Mn^{2+} is enthalpically less unfavorable causing the binding of the second manganese cation to an already formed complex to be an exothermic process. Entropic gain is somewhat lower for this complex, resulting in a slightly greater stepwise equilibrium constant for the binding of the second Mn^{2+} cation. This finding indicates a weak allosteric effect of the Mn^{2+} binding. Most likely the binding of the first cation results in favorable preorganization of the protein for tighter binding of the next cation. An analogous conclusion can be drawn for the complex containing 4 cations, as the related logβ is 4.1 times larger than the log$K$ for the $ScaR_2Mn$ complex. Namely, a significant decrease in the successive constant is expected due to statistical effects if the binding of each cation is independent. This observation is consistent with previous studies which have shown that the ancillary binding site has a higher affinity for transition metal ion binding than the primary binding site [8,9,45,46]. Some discrepancies in the ITC curve compared to the one previously reported by Stoll et al. are most likely caused by variations in the conditions used (ionic strength, presence of glycerol).

Based on the collected equilibrium constants the distribution diagram for the system containing Mn^{2+} and $ScaR_2$ could be calculated (Fig. 9). The $ScaR_2Mn_4$ complex predominates throughout the best part of the titration, as soon as more than two equivalents of Mn^{2+} are added. As already stated, the monocationic complex is present in the solution in a substantial fraction only at relatively low Mn:$ScaR_2$ ratio, competing with the $ScaR_2Mn_2$ complex.

To further study the binding ratio of Mn^{2+}ions to the ScaR protein, EPR measurements were performed. The obtained EPR spectra of Mn^{2+} in the buffer in the presence and absence of ScaR are presented in Fig. 10. The isotropic signals centered at $g \approx 2$ acquired at room temperature are typical for $Mn(H_2O)_6^{2+}$ exhibiting 6 lines due to the hyperfine interaction of electron spins with the ^{55}Mn nuclei bearing spin 5/2. It can be easily noticed that only the signal intensity changes in the presence of protein. It should be noted that upon binding of Mn^{2+} to the protein only the EPR signal of unbound Mn^{2+} in the solvent can be detected [47]. Therefore, a decrease of the EPR signal in the buffer solution in the presence of protein implies the binding of Mn^{2+} to protein ScaR. Comparing the EPR spectra of Mn^{2+} in the solution in the presence and absence of protein one can estimate the binding of roughly two manganese ions per protein monomer *i.e.*, that the $ScaR_2Mn_4$ complex predominates in solution at the experimentally applied conditions.

These observations are consistent with previous functional studies on ScaR protein which indicate that two to three Mn^{2+} ions per monomer are required for activation [9,12]. So far there is no crystal structure of ScaR in its Mn^{2+}-bound form, but crystal structures of Zn^{2+}- and Cd^{2+}- bound ScaR, where the metal ions are positioned in the secondary binding site, were reported. The secondary binding site is formed by ligand residues Glu80, Cys123 and His125 [9,13]. Although the known structures point to the possibility of transition metal binding in the secondary binding site with the sulfur containing ligand residue Cys123, there are no known proteins selective for Mn^{2+} ions that use sulfur atoms as ligands [18,19]. For this reason, the possibility of Mn^{2+} ion binding in the secondary binding site is not likely, which additionally explains why four, and not six, Mn^{2+} ions bind to ScaR. Because of this, it can be concluded that it is most likely that the four Mn^{2+}ions bind to the primary and ancillary binding sites of dimer ScaR which consist of Glu, Asp and His ligand residues.

4. Conclusion

Our results (both computational and experimental) point to binding of two, and not three, Mn^{2+} ions per monomer of ScaR protein. Of these, the first one binds in the ancillary site (higher binding affinity), and the second one to the primary site. We have further shown that binding in the primary binding site alone is enough to induce conformational change in the protein – drawing closer of DBD domains, thus enabling their binding to DNA. Together with significant stabilization of protein upon binding of Mn^{2+} ions, these results represent solid basis for further research, not only on ScaR mechanism of action, but also on its counterpart from cariogenic bacterium, SloR.

Funding

This research was funded by the Croatian Science Foundation, grant number IP-2020-02-3446.

CRediT authorship contribution statement

Katarina Radman : Investigation, Writing – original draft, Writing – review & editing, Formal analysis, Visualization. **Zoe Jelić Matošević :** Investigation. **Dijana Žilić :** Investigation. **Ivo Crnolatac :** Investigation. **Nikola Bregović :** Investigation, Writing – review & editing. **Marina Kveder :** Investigation. **Ivo Piantanida :** Supervision. **Pedro A. Fernandes :** Investigation, Supervision. **Ivana Leščić Ašler :** Investigation, Supervision, Writing – review & editing. **Branimir Bertoša :** Conceptualization, Supervision, Writing – original draft, Writing – review & editing, Project administration, Funding acquisition.

Declaration of competing interest

The authors declare that they have no known competing financial interests or personal relationships that could have appeared to influence the work reported in this paper.

Acknowledgments

We acknowledge the **Croatian Science Foundation** for funding, grant number IP-2020-02-3446, grant title "Manganese metallosensors". We thank the **Zagreb University Computing Centre** (SRCE) for providing computational resources available at computer cluster Isabella. We thank **Rui P. P. Neves** from the Department of Chemistry and Biochemistry, Faculty of Science, University of Porto, for the help in the parametrization of the metallocentres in ScaR protein.

Appendix A. Supplementary data

Supplementary data to this article can be found online at https://doi.org/10.1016/j.ijbiomac.2023.127572.

References

[1] N.S. Jakubovics, S.A. Yassin, A.H. Rickard, Community interactions of oral streptococci, Adv. Appl. Microbiol. 87 (2014) 43–110, https://doi.org/10.1016/B978-0-12-800261-2.00002-5.
[2] J. Abranches, L. Zeng, J.K. Kajfasz, S.R. Palmer, B. Chakraborty, Z.T. Wen, et al., Biology of oral streptococci, Microbiol. Spectr. (2018) 6, https://doi.org/10.1128/MICROBIOLSPEC.GPP3-0042-2018.
[3] N. Mosailova, J. Truong, T. Dietrich, J. Ashurst, Streptococcus gordonii: a rare cause of infective endocarditis, Case Rep. Infect. Dis. 2019 (2019) 1–2, https://doi.org/10.1155/2019/7127848.
[4] C.R. Back, M.N. Sztukowska, M. Till, R.J. Lamont, H.F. Jenkinson, A.H. Nobbs, et al., The Streptococcus gordonii adhesin CshA protein binds host fibronectin via a catch-clamp mechanism, J. Biol. Chem. 292 (2017) 1538–1549, https://doi.org/10.1074/jbc.M116.760975.
[5] P.E. Kolenbrander, R.N. Andersen, R.A. Baker, H.F. Jenkinson, The adhesion-associated sca operon in Streptococcus gordonii encodes an inducible high-affinity ABC transporter for Mn2+ uptake, J. Bacteriol. 180 (1998) 290–295, https://doi.org/10.1128/JB.180.2.290-295.1998.
[6] H.F. Jenkinson, R.J. Lamont, Streptococcal adhesion and colonization, Crit. Rev. Oral Biol. Med. 8 (1997) 175–200, https://doi.org/10.1177/10454411970080020601.
[7] O.J. Park, Y. Kwon, C. Park, Y.J. So, T.H. Park, S. Jeong, et al., Streptococcus gordonii: pathogenesis and host response to its cell wall components, Microorganisms 8 (2020) 1–22, https://doi.org/10.3390/MICROORGANISMS8121852.
[8] N.S. Jakubovics, A.W. Smith, H.F. Jenkinson, Expression of the virulence-related Sca (Mn2+) permease in Streptococcus gordonii is regulated by a diphtheria toxin metallorepressor-like protein ScaR, Mol. Microbiol. 38 (2000) 140–153, https://doi.org/10.1046/J.1365-2958.2000.02122.X.
[9] K.E. Stoll, W.E. Draper, J.I. Kliegman, M.V. Golynskiy, R.A.T. Brew-Appiah, R.K. Phillips, et al., The characterization and structure of the manganese-responsive transcriptional regulator ScaR, Biochemistry 48 (2009) 10308, https://doi.org/10.1021/BI900980G.
[10] D.A. Capdevila, K.A. Edmonds, D.P. Giedroc, Metallochaperones and metalloregulation in bacteria, Essays Biochem. 61 (2017) 177, https://doi.org/10.1042/EBC20160076.
[11] S. Aggarwal, M. Kumaraswami, Managing manganese: the role of manganese homeostasis in streptococcal pathogenesis, Front. Cell Dev. Biol. 10 (2022) 1307, https://doi.org/10.3389/FCELL.2022.921920.
[12] J.W. Johnston, D.E. Briles, L.E. Myers, S.K. Hollingshead, Mn2+-dependent regulation of multiple genes in Streptococcus pneumoniae through PsaR and the resultant impact on virulence, Infect. Immun. 74 (2006) 1171, https://doi.org/10.1128/IAI.74.2.1171-1180.2006.
[13] P. Monette, R. Brach, A. Cowan, R. Winters, J. Weisman, F. Seybert, et al., Autoregulation of the Streptococcus mutans SloR metalloregulator is constitutive and driven by an independent promoter, J. Bacteriol. 200 (2018) 214–232, https://doi.org/10.1128/JB.00214-18.
[14] H. Do, N. Makthal, P. Chandrangsu, R.J. Olsen, J.D. Helmann, J.M. Musser, et al., Metal sensing and regulation of adaptive responses to manganese limitation by MtsR is critical for group A streptococcus virulence, Nucleic Acids Res. 47 (2019) 7476, https://doi.org/10.1093/NAR/GKZ524.
[15] J.A. D'Aquino, J. Tetenbaum-Novatt, A. White, F. Berkovitch, D. Ringe, Mechanism of metal ion activation of the diphtheria toxin repressor DtxR, Proc. Natl. Acad. Sci. U. S. A. 102 (2005) 18408–18413, https://doi.org/10.1073/PNAS.0500908102/ASSET/B4641111-B292-4F59-BDA5-6D65BC195BD5.
[16] E. Pohl, R.K. Holmes, W.G.J. Hol, Crystal structure of a cobalt-activated diphtheria toxin repressor-DNA complex reveals a metal-binding SH3-like domain, J. Mol. Biol. 292 (1999) 653–667, https://doi.org/10.1006/JMBI.1999.3073.
[17] G. Spatafora, J. Corbett, L. Cornacchione, W. Daly, D. Galan, M. Wysota, et al., Interactions of the metalloregulatory protein SloR from Streptococcus mutans with its metal ion effectors and DNA binding site, J. Bacteriol. 197 (2015) 3601–3615, https://doi.org/10.1128/JB.00612-15.
[18] E. Guedon, J.D. Helmann, Origins of metal ion selectivity in the DtxR/MntR family of metalloregulators, Mol. Microbiol. 48 (2003) 495–506, https://doi.org/10.1046/J.1365-2958.2003.03445.X.
[19] M.M. Harding, The geometry of metal-ligand interactions relevant to proteins, Acta Crystallogr. D Biol. Crystallogr. 55 (1999) 1432–1443, https://doi.org/10.1107/S0907444999007374.
[20] A. Waterhouse, M. Bertoni, S. Bienert, G. Studer, G. Tauriello, R. Gumienny, et al., SWISS-MODEL: homology modelling of protein structures and complexes, Nucleic Acids Res. 46 (2018) W296–W303, https://doi.org/10.1093/nar/gky427.
[21] The PyMOL Molecular Graphics System n.d.
[22] R. Anandakrishnan, B. Aguilar, A.V. Onufriev, H++ 3.0: automating pK prediction and the preparation of biomolecular structures for atomistic molecular modeling and simulations, Nucleic Acids Res. 40 (2012) W537–W541, https://doi.org/10.1093/nar/gks375.
[23] S. Baliga, S. Muglikar, R. Kale, Salivary pH: a diagnostic biomarker, J. Indian Soc. Periodontol. 17 (2013) 461, https://doi.org/10.4103/0972-124X.118317.
[24] W.R. Pearson, D.J. Lipman, Improved tools for biological sequence comparison, Proc. Natl. Acad. Sci. 85 (1988) 2444–2448, https://doi.org/10.1073/PNAS.85.8.2444.
[25] S. Zheng, Q. Tang, J. He, S. Du, S. Xu, C. Wang, et al., VFFDT: a new software for preparing AMBER force field parameters for metal-containing molecular systems, J. Chem. Inf. Model. 56 (2016) 811–818, https://doi.org/10.1021/ACS.JCIM.5B00687/.
[26] U.C. Singh, P.A. Kollman, An approach to computing electrostatic charges for molecules, J. Comput. Chem. 5 (1984) 129–145, https://doi.org/10.1002/JCC.540050204.
[27] W.D. Cornell, P. Cieplak, C.I. Bayly, P.A. Kollman, Application of RESP charges to calculate conformational energies, hydrogen bond energies, and free energies of solvation, J. Am. Chem. Soc. 115 (1993) 9620–9631, https://doi.org/10.1021/JA00074A030.
[28] P. Li, B.P. Roberts, D.K. Chakravorty, K.M. Merz, Rational design of particle mesh ewald compatible lennard-jones parameters for +2 metal cations in explicit solvent, J. Chem. Theory Comput. 9 (2013) 2733–2748, https://doi.org/10.1021/CT400146W/SUPPL_FILE/CT400146W_SI_003.XLSX.
[29] D.A. Case, K. Belfon, I.Y. Ben-Shalom, S.R. Brozell, D.S. Cerutti, T.E. Cheatham, I.I.I. VWDC, T.A. Darden, R.E. Duke, G. Giambasu, M.K. Gilson, H. Gohlke, A.W. Goetz, R. Harris, S. Izadi, S.A.I. Mailov, K. Kasavajhala, A. Kovalenko, R. Krasny, T. Kurtzman, T.S. Lee, S. LeGrand, P. Li, C. Lin JL, T. Luchko, R. Luo, V. Man, K.M. Merz, Y. Miao, O. Mikhailovskii, G. Monard, H. Nguyen, A. Onufriev F, S. Pantano Pan, R. Qi, D.R. Roe, A. Roitberg, C. Sagui, S. Schott-Verdugo, J. Shen, C.L. Simmerling NR, J. Smith Skrynnikov, J. Swails, R.C. Walker, J. Wang, L. Wilson, R.M. Wolf, X. Wu, Y. Xiong YX, et al., AMBER 2020, 2020.
[30] R. Salomon-Ferrer, A.W. Götz, D. Poole, S. le Grand, R.C. Walker, Routine microsecond molecular dynamics simulations with AMBER on GPUs. 2. Explicit solvent particle mesh Ewald, J. Chem. Theory Comput. 9 (2013) 3878–3888, https://doi.org/10.1021/CT400314Y.
[31] A.W. Götz, M.J. Williamson, D. Xu, D. Poole, S. Le Grand, R.C. Walker, Routine microsecond molecular dynamics simulations with AMBER on GPUs. 1. Generalized born, J. Chem. Theory Comput. 8 (2012) 1542–1555, https://doi.org/10.1021/CT200909J.
[32] S. le Grand, A.W. Götz, R.C. Walker, S. le Grand, A.W. Götz, R.C. Walker, SPFP: speed without compromise—a mixed precision model for GPU accelerated molecular dynamics simulations, CoPhC 184 (2013) 374–380, https://doi.org/10.1016/J.CPC.2012.09.022.
[33] R.J. Loncharich, B.R. Brooks, R.W. Pastor, Langevin dynamics of peptides: the frictional dependence of isomerization rates of N-acetylalanyl-N′-methylamide, Biopolymers 32 (1992) 523–535, https://doi.org/10.1002/BIP.360320508.

[34] U. Essmann, L. Perera, M.L. Berkowitz, T. Darden, H. Lee, L.G. Pedersen, A smooth particle mesh Ewald method, J. Chem. Phys. 103 (1998) 8577, https://doi.org/10.1063/1.470117.
[35] RStudio Team, RStudio: Integrated Development Environment for R, 2020.
[36] M. Dowle, A. Srinivasan, data.table: Extension of 'data.frame', 2021.
[37] H. Wickham, ggplot2: Elegant Graphics for Data Analysis, Springer-Verlag, New York, 2016.
[38] W. Humphrey, A. Dalke, K. Schulten, VMD: Visual molecular dynamics, J. Mol. Graph. 14 (1996) 33–38, https://doi.org/10.1016/0263-7855(96)00018-5.
[39] Maestro | Schrödinger, n.d. https://www.schrodinger.com/products/maestro. (Accessed 14 March 2023).
[40] GitHub - matkozic/TrajMap: MD simulation trajectory visualization tool, n.d. https://github.com/matkozic/TrajMap. (Accessed 14 March 2023).
[41] F.J. Marcos-Torres, D. Maurer, L. Juniar, J.J. Griese, The bacterial iron sensor IdeR recognizes its DNA targets by indirect readout, Nucleic Acids Res. 49 (2021) 10120–10135, https://doi.org/10.1093/NAR/GKAB711.
[42] E. Gasteiger, C. Hoogland, A. Gattiker, S. Duvaud, M.R. Wilkins, R.D. Appel, et al., The Proteomics Protocols Handbook. The Proteomics Protocols Handbook, 2005, pp. 571–607, https://doi.org/10.1385/1592598900.
[43] A. Micsonai, É. Moussong, F. Wien, E. Boros, H. Vadászi, N. Murvai, et al., BeStSel: webserver for secondary structure and fold prediction for protein CD spectroscopy, Nucleic Acids Res. 50 (2022) W90–W98, https://doi.org/10.1093/NAR/GKAC345.
[44] S.A. Lieser, T.C. Davis, J.D. Helmann, S.M. Cohen, DNA-binding and oligomerization studies of the manganese(II) metalloregulatory protein MntR from Bacillus subtilis, Biochemistry 42 (2003) 12634–12642, https://doi.org/10.1021/BI0350248.
[45] C.S. Bates, C. Toukoki, M.N. Neely, Z. Eichenbaum, Characterization of MtsR, a new metal regulator in group A Streptococcus, involved in Iron acquisition and virulence, Infect. Immun. 73 (2005) 5743, https://doi.org/10.1128/IAI.73.9.5743-5753.2005.
[46] E. Rolerson, A. Swick, L. Newlon, C. Palmer, Y. Pan, B. Keeshan, et al., The SloR/Dlg metalloregulator modulates Streptococcus mutans virulence gene expression, J. Bacteriol. 188 (2006) 5033–5044, https://doi.org/10.1128/JB.00155-06.
[47] K.I. Sen, A. Sienkiewicz, J.F. Love, J.C. VanderSpek, P.G. Fajer, T.M. Logan, Mn (II) binding by the anthracis repressor from Bacillus anthracis, Biochemistry 45 (2006) 4295–4303, https://doi.org/10.1021/BI052288G.